Investigation on the Influence of Structural Parameters of Parallel Reactant Flow Channels on the Heat Transfer Characteristics of Bipolar Plates for Hydrogen Fuel Cells in UAV Applications

Jiren Li[1], Lei Xi[1,*], Yunlong Zhou[1], Jianmin Gao[1], Liang Xu[1], Tao Yang[2] and Zelin Zhi[2]

[1]*School of Mechanical Engineering, Xi'an Jiaotong University, Xi'an 710049, Shaanxi, China*

[2]*Shaanxi Special Equipment Inspection and Testing Institute, Xi'an 710048, Shaanxi, China*

Abstract: This study investigates a 20 kW hydrogen fuel cell for Unmanned Aerial Vehicle (UAV) applications, employing numerical simulations to analyze the influence of structural parameters within parallel reactant flow channels on the heat transfer characteristics of the bipolar plates. The effects of variations in channel width, height, and spacing on thermal performance were examined. Key thermal metrics, including the maximum, average, and minimum temperatures, as well as the temperature difference across the bipolar plates, were systematically evaluated under different channel configurations. The results reveal a significant non-uniformity in the temperature distribution of the fuel cell. Lower temperatures were observed near the reactant inlets and along the sides of the cell, while a triangular high-temperature zone formed adjacent to the reactant outlets. As the channel width ratio increased from 0.02 to 0.04, the maximum and average cell temperatures initially rose and then decreased, peaking at a width ratio of 0.03. At this specific ratio, the temperature difference within the reactant channels was minimized, whereas it reached a maximum within the cooling channels. The overall system temperature difference attained its peak value near a width ratio of 0.035. In contrast, variations in the channel height ratio and spacing ratio were found to have a negligible impact on the core temperature of the fuel cell but significantly influenced the temperature distribution within the cooling channels. Under all tested height and spacing ratios, the temperature difference in the cathode cooling channel (approximately 8 K max.) consistently exceeded that in the anode cooling channel (approximately 2 K max.). The findings of this study provide valuable insights for the design of reactant flow channels in bipolar plates for UAV-oriented hydrogen fuel cells, thereby providing critical technical support for enhancing UAV flight safety assurance, endurance enhancement, sustainable flight efficiency, and overall operational reliability.

Keywords: Hydrogen-powered UAV, Fuel Cell, Bipolar Plates, Reactant Flow Channels, Heat Transfer Characteristics.

1. INTRODUCTION

With the accelerated development of intelligent aviation systems and sustainable aviation technologies, the global aviation industry is imposing unprecedented high standards on power sources concerning power density, environmental adaptability, and operational reliability. Hydrogen fuel cell systems, characterized by their cleanliness and high efficiency, represent a critical technological pathway towards achieving long-endurance and sustainable flight, establishing them as an ideal choice for powering long-endurance unmanned aerial vehicles (UAVs). However, under extreme operating conditions encountered by UAVs, such as high altitude, low pressure, and high-power climbs, a prominent challenge emerges: a significant increase in system heat generation occurs concurrently with a decrease in heat dissipation efficiency. This severe thermal management issue directly poses a critical challenge to flight safety assurance, endurance enhancement, sustainable flight efficiency, and overall operational reliability of UAVs.

As the core of the hydrogen fuel cell system, the Proton Exchange Membrane Fuel Cell (PEMFC) converts approximately 50% of the hydrogen's chemical energy into heat during operation [1]. This implies that without efficient thermal management, a substantial amount of waste heat accumulates within the stack, leading to localized hot spots and significant temperature gradients. These conditions can cause catalyst deactivation and membrane dehydration, and in severe cases, may even trigger thermal runaway [2]. Studies indicate that temperature fluctuations exceeding 5°C can result in more than 10% performance degradation [3]. Therefore, achieving efficient and uniform heat dissipation is paramount for ensuring the longevity and safety of hydrogen fuel cells.

Current research on hydrogen fuel cell thermal management primarily focuses on the structural design of cooling flow channels, the structural design of reactant flow channels, and numerical models for internal heat and mass transfer.

In the realm of cooling flow channel design, researchers have developed various configurations to achieve efficient cooling, including parallel, pin-type,

---

*Address correspondence to this author at the School of Mechanical Engineering, Xi'an Jiaotong University, Xi'an 710049, Shaanxi, China; E-mail: xilei100@mail.xjtu.edu.cn

serpentine, multi-pass serpentine, and spiral flow fields [4]. Sasmto *et al*. [5] numerically compared the cooling performance of different cooling channel geometries. Afshari *et al*. [6] compared temperature parameters between zigzag and straight channel models, finding that the thermal performance improvement of zigzag channels was more pronounced at higher coolant flow rates and heat loads. Joibary *et al*. [7] investigated four different cooling flow field layouts, discovering that a parallel geometry achieved the optimal pressure drop under identical coolant mass flow rates, whereas a four-pass serpentine design performed the worst. Li *et al*. [8] numerically studied the thermal performance of cooling plates with conventional straight channels and wavy channels. Their results showed that wavy channels significantly enhanced cooling performance, albeit with a substantial increase in pressure drop. Peng *et al*. [9] confirmed that the single-serpentine flow field yielded better performance under normal pressure, but its cathode pressure drop was considerably larger than that of the parallel flow field.

Regarding reactant flow channel design, research on flow field structures has been ongoing since the inception of fuel cells. Common configurations include serpentine, parallel, interdigitated, mesh, spiral, and blocked-assisted channels [10]. Related studies primarily aim to optimize mass transfer and reaction efficiency within the fuel cell, thereby enhancing performance, by modifying channel shape, dimensions, and layout [11]. Shen *et al*. [12] provided a detailed investigation of fuel cell performance with parallel, single-serpentine, and pressured parallel flow fields. Their findings indicated that the single-serpentine flow field offered superior performance under normal pressure. Liao *et al*. [13] proposed a zigzag flow field with alternating positive and negative permutations based on the parallel flow field. Their research found that this structure reduced mass transfer resistance and promoted more uniform distributions of oxygen, water content, temperature, and current density. Najmi *et al*. [14] analyzed and compared wavy, serpentine, interdigitated, and parallel flow fields, conducting performance tests at 40%, 60%, and 80% relative humidity and analyzing polarization curves and electrochemical impedance. Alizadeh *et al*. [15] studied a novel series multi-serpentine flow field, investigating the effects of channel width, rib width, and channel depth on fuel cell performance. The results demonstrated that the novel flow field significantly mitigated water flooding and improved water distribution uniformity compared to traditional serpentine channels. Furthermore, other improved flow field structures, such as alternating flow fields [16], blocked channels [17], wavy channels [18], and baffles [19], have been developed to enhance gas supply efficiency and temperature distribution. Beyond conventional structures, bio-inspired flow fields are also being applied to the cathode to improve reaction efficiency [20].

Concerning numerical models for internal heat and mass transfer, the focus is on investigating and analyzing the distribution of reactive gases, water, and temperature across the proton exchange membrane. These models can be categorized by dimensionality: one-dimensional (1D), two-dimensional (2D), and three-dimensional (3D). Early research predominantly employed 1D and 2D models. With the rapid advancement of Computational Fluid Dynamics (CFD), 3D numerical simulation has become a crucial means for modeling the entire operational process of fuel cells. Atyabi *et al*. [21] developed a 3D multiphase model accounting for contact resistance between the Gas Diffusion Layer (GDL) and the current collector to evaluate the performance of an open-cathode fuel cell with external cooling channels. The results showed that adding cooling channels enhanced the cooling capacity, reduced stack temperature, alleviated water retention, and stabilized proton transfer across the membrane, thereby improving fuel cell performance. Carcadea *et al*. [22] indicated that appropriately reducing GDL thickness or increasing GDL porosity improved the diffusion efficiency of reactive gases and water transport capability within the cell, enhancing output performance. Shen *et al*. [23] found that cells operating under conditions of high reactant gas humidity and high current density exhibited the highest internal water content and the poorest uniformity of water distribution, leading to severe performance degradation over prolonged operation. Peng *et al*. [24] established a 3D transient heat and mass transfer model for a fuel cell with a closed flow field structure, analyzing the transient behavior during startup and shutdown under different operating parameters. Chen *et al*. [25] proposed a steady-state numerical model for a fuel cell containing 3D wavy flow channels, investigating the effect of channel geometry on the distribution of reactive gases and water/thermal fields. Atyabi *et al*. [26] found that a novel honeycomb flow field reduces membrane water content while improving the uniformity of temperature, pressure, and reactant distributions, which collectively mitigates risks of local hot spots and flooding of fuel cells.

However, the reactant flow channels not only serve to transport fuel and oxidant but also significantly influence the overall temperature distribution within the cell through their flow and convective heat transfer processes. In particular, the structural parameters of these reactant channels also impact the overall thermal performance of the fuel cell—a significant gap that has not yet received adequate attention in current research concerning UAV thermal management and sustainable flight technologies. Therefore, addressing the urgent demands of sustainable flight technology for power systems with high thermal stability, safety, reliability, and long endurance, this study focuses on a 20kW hydrogen fuel cell for UAV applications. Utilizing numerical simulation, the impact of structural parameters—specifically width, height, and spacing—of parallel reactant flow channels on the heat transfer characteristics of the bipolar plates was thoroughly investigated. The analysis examines how these variations affect key thermal performance metrics, including the temperature distribution at the interface between the Proton Exchange Membrane and the Cathode Catalyst Layer, the overall maximum, average, and minimum temperatures, the overall temperature difference, and the temperature differences within individual channels. The innovation of this work lies in revealing the influence of reactant channel structural parameters on the thermal distribution characteristics of hydrogen fuel cells, thereby filling a critical research gap in the relationship between the architecture of the reactant flow field and the resultant thermal performance of hydrogen fuel cells. The findings in this study may provide valuable insights for the design of reactant flow channels in bipolar plates for UAV hydrogen fuel cells, thereby providing critical technical support for enhancing UAV flight safety assurance, endurance enhancement, sustainable flight efficiency, and overall operational reliability.

2. RESEARCH SUBJECT

This study focuses on a 20kW hydrogen fuel cell for Unmanned Aerial Vehicle (UAV) applications. The structure of a typical fuel cell single cell is depicted in Figure **1a**. To facilitate numerical simulation and analysis, the original single-cell model was appropriately simplified. The simplified computational model is presented in Figure **1b**, a schematic diagram illustrating its key structural parameters is shown in Figure **1c**, and the corresponding values of these fundamental structural parameters are summarized in Table **1**.

To investigate the influence of reactant channel structural parameters on the heat transfer characteristics of the bipolar plates, this study systematically varied the channel width, height, and spacing, as detailed below:

Specifically, the ratio of the reactant channel width (w_1) to the membrane electrode assembly (MEA) width (W), defined as w_1/W, was varied within the range of 0.02 to 0.04. The ratio of the reactant channel depth (h_1) to the current collector height (H), denoted as h_1/H, was adjusted from 0.25 to 0.35. Furthermore, the ratio of the spacing between adjacent reactant channels (Δ_1) to the MEA width (W), expressed as Δ_1/W, was modified across the range of 0.02 to 0.024.

During the investigation, a controlled variable approach was employed: while two of the three structural parameters were held constant, the third parameter was altered at equal intervals. This methodology resulted in a total of 13 distinct simulation cases. The specific parameter combinations for these cases are provided in Table **2**.

3. RESEARCH METHODOLOGY

3.1. Numerical Model and Methods

A three-dimensional multiphysics coupling simulation model was employed to simulate the Hydrogen Fuel Cell in this study, with subsequent analysis and evaluation of the results. Figure **2** illustrates the schematic of the numerical model for the single cell.

In the simulation setup, the flow channels are treated as fluid domains. Within these regions, the transport of electrons and protons is not considered. The primary physical processes encompass fluid flow, heat transfer, and species transport. Consequently, the governing equations for this domain include the mass, momentum, and energy conservation equations for the gas mixtures, the species conservation equations for the reactant gases (hydrogen and oxygen), and a model for liquid water transport. Furthermore, as the flow channel region contains inlet and outlet boundaries, appropriate boundary conditions describing the inlet flows and outlet pressures are applied.

The current collector regions are treated as solid domains. Serving as the bridge to the external circuit, these regions involve the transport of electrons and heat conduction. Therefore, the model incorporates the

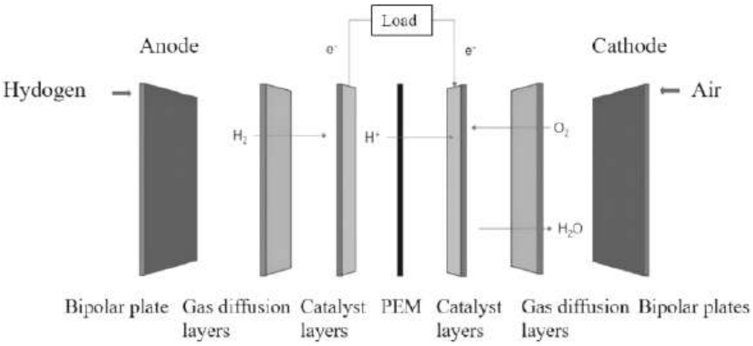

(a) Structure of the single-cell fuel cell

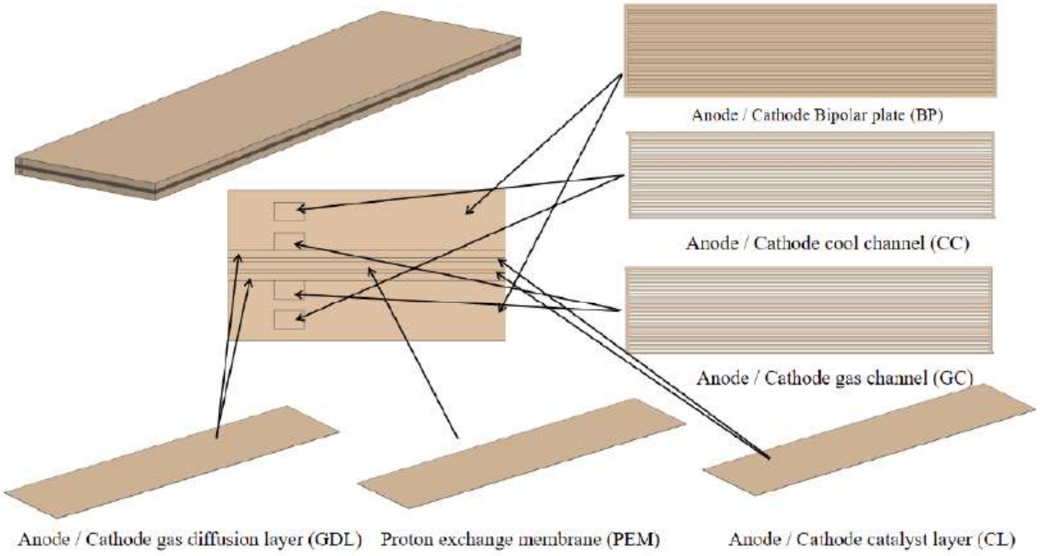

(b) Simplified model of the single-cell fuel cell

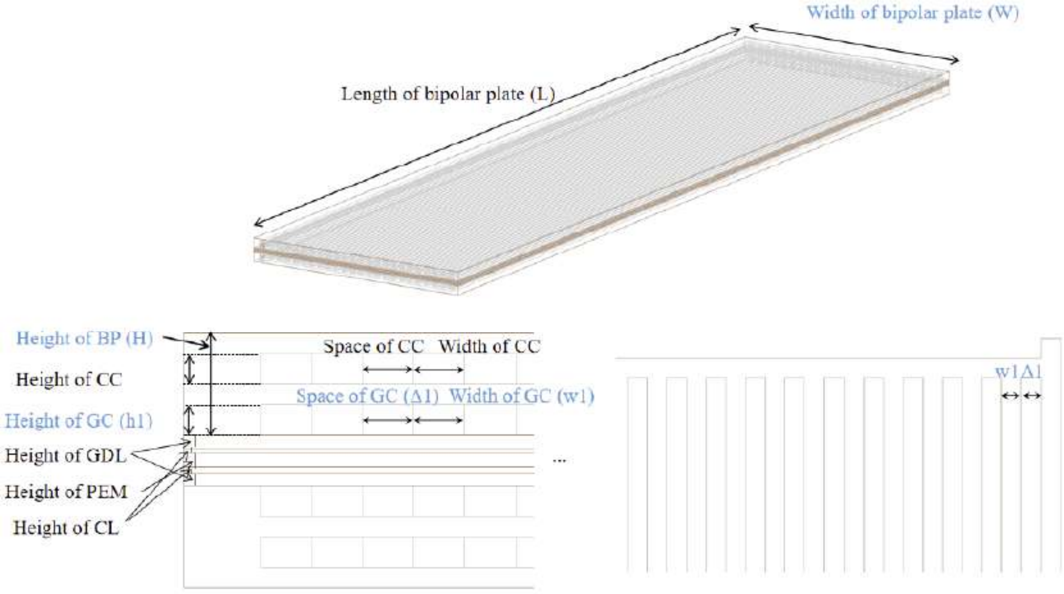

(c) Schematic diagram of the single-cell structural parameters

Figure 1: Research subject.

Table 1: Basic Structural Parameters of the Single Cell

Parameters	Dimensions (mm)
Membrane electrode length	200
Membrane electrode width	50
Collector plate height	4
Diffusion layer thickness	0.5
Catalytic layer thickness	0.25
Proton exchange membrane thickness	0.5

Table 2: Calculation Arrangement for the Influence of Reactant Channel Structure Parameters

Case	w1/W	h1/H	Δ1/W
1	0.02	0.3	0.02
2	0.025	0.3	0.02
3	0.03	0.3	0.02
4	0.035	0.3	0.02
5	0.04	0.3	0.02
6	0.02	0.25	0.02
7	0.02	0.275	0.02
8	0.02	0.325	0.02
9	0.02	0.35	0.02
10	0.02	0.3	0.016
11	0.02	0.3	0.018
12	0.02	0.3	0.022
13	0.02	0.3	0.024

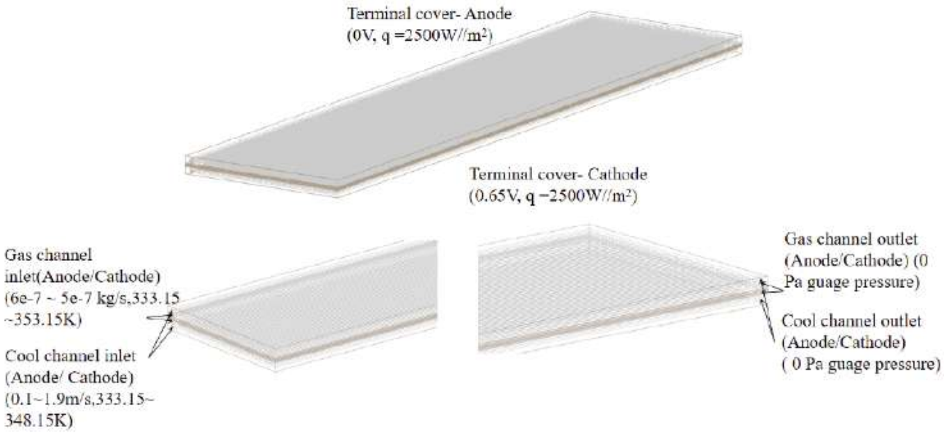

Figure 2: Schematic diagram of numerical calculation model.

respective governing equations for these processes and applies corresponding electrical potential and thermal boundary conditions.

In summary, the computational domain is partitioned according to the physical components. The involved electrochemical reactions, namely the hydrogen oxidation reaction and the oxygen reduction reaction, occur in distinct regions (the anode and cathode catalyst layers, respectively). Similarly, the physical processes, such as proton transport through

Table 3: Material Parameters

Components	Physical property parameters	Values	Units
Bipolar plate	material density	2160	$kg\cdot m^{-3}$
	specific heat capacity	610	$J\cdot kg^{-1}\cdot K^{-1}$
	conductivity	92600	$\Omega^{-1}\cdot m^{-1}$
	thermal conductivity	129	$W\cdot m^{-1}\cdot K^{-1}$
	modulus of elasticity	1E10	MPa
	Poisson's ratio	0.25	\
	coefficient of thermal expansion	7.6E-6	\
Diffusion layer	material density	450	$kg\cdot m^{-3}$
	conductivity	280	$\Omega^{-1}\cdot m^{-1}$
	porosity	0.6	m^{-2}
	permeability	1.76E-11	Pa
	modulus of elasticity	6.13E6	\
	Poisson's ratio	0.09	\
	coefficient of thermal expansion	1.7E-6	\
Catalytic layer	porosity	0.4	\
	permeability	1.76E-11	m^{-2}
	specific surface area	1.127E7	$7m^{-1}$
Proton exchange membrane	thermal conductivity	2	$W\cdot m^{-1}\cdot K^{-1}$
	Dry film density	1980	$kg\cdot m^{-3}$
	Equivalent mass of dry film	1100	$kg\cdot kmol^{-1}$
	modulus of elasticity	8.5E7	7Pa
	Poisson's ratio	0.3	\
	coefficient of thermal expansion	1.23E-4	

the membrane and the transport of gaseous/liquid water, differ across these subdomains. Accurately describing the corresponding governing equations for each region is therefore essential to numerically replicate the operational behavior of a Hydrogen Fuel Cell. The formulation of these governing equations involves numerous material parameters. The material parameters selected for the Hydrogen Fuel Cell components in this study are summarized in Table **3**.

In the numerical simulation, the governing equations—namely, the mass, momentum, and energy conservation equations—were discretized using a finite-element-based finite difference method [27]. The three-dimensional, compressible Reynolds-Averaged Navier-Stokes (RANS) equations were solved using ANSYS Fluent 19.2 software, employing a fully implicit coupled multigrid approach. Diffusion, source, and convection terms within the equations were discretized using high-precision schemes.

Given that a hydrogen fuel cell constitutes a complex, three-dimensional, multiphase, multi-scale, and dynamic system, the numerical model in this study was founded upon the following simplifying assumptions:

1) The fuel cell operates under steady-state, non-isothermal, and multi-component conditions.

2) All gas phases are treated as ideal gases, and the influence of gravity is neglected.

3) Gas permeation through the proton exchange membrane is considered negligible.

4) The flow within the channels is assumed to be laminar.

5) All layers within the fuel cell are considered isotropic and homogeneous.

Consequently, the corresponding Fuel Cell module in ANSYS Fluent 19.2 was activated, alongside the laminar flow model and the species transport model.

The physical phenomena occurring within a hydrogen fuel cell can generally be described by solutions to the conservation equations of momentum, mass, and energy. Furthermore, due to the interactions between multiple chemical species, the species conservation equation must also be satisfied. Therefore, the specific governing equations implemented in the numerical model are as follows:

The conservation equations of continuity, energy and momentum are as follows:

$$\frac{\partial(\varepsilon\rho)}{\partial t}+\square(\varepsilon\rho v)=S_{\mathrm{mass}} \tag{1}$$

$$\frac{\partial(\varepsilon\rho c_p T)}{\partial t}+\square\left(\varepsilon\rho c_p vT\right)=\square\left(k^{\mathrm{eff}}\square T\right)+S_e \tag{2}$$

$$\frac{1}{\varepsilon^2}\square(\rho v)=-\square p+\left(k^{\mathrm{eff}}\square v\right)+S_{\mathrm{mom}} \tag{3}$$

where p is pressure; v is kinematic viscosity; c_p is specific heat at constant pressure; T is temperature; k^{eff} is effective thermal conductivity; S_e is the energy source term; S_{mom} is the source term of momentum.

The conservation equation of components:

$$\frac{\partial(\varepsilon c_i)}{\partial t}+\square(\varepsilon v c_i)=\square(D_i^{\mathrm{eff}}\square c_i)+S_i \tag{4}$$

where c_i is component concentration; D_i^{eff} is effective diffusion coefficient of components; S_i is energy source term; i is the meaning of the anode in a battery is hydrogen and water vapor, while the meaning of the cathode in a battery is oxygen and water vapor.

The charge conservation equation:

$$\square\square(\sigma^{eff}\square\varphi)+S_{\varphi}=0 \tag{5}$$

where σ^{eff} is electrical conductivity; φ is electric potential; S_{φ} is current source term.

3.2. Boundary Conditions

As illustrated in Figure **2**, the overall geometry of the model is a rectangular cuboid containing multiple internal channels and various plate surfaces. The anode bipolar plate surface was set to an electric potential of 0 V and subjected to a heat flux of 2500 W/m². At the cooling channel inlet, the coolant velocity was controlled within a range of 0.1 to 1.9 m/s, and its temperature was maintained between 333.15 K and 348.15 K. The anode and cathode reactant channel inlets were assigned mass flow rates ranging from 6×10^{-7} to 5×10^{-6} kg/s, with inlet temperatures also specified within the 333.15 K to 348.15 K range. A static back pressure of 0 Pa (gauge pressure) was prescribed at the outlets of both the cooling and reactant channels. Furthermore, backflow suppression was enabled at these outlets to ensure unidirectional flow and prevent potential numerical inaccuracies associated with flow reversal. The cathode bipolar plate surface was set to an electric potential of 0.65 V, with an applied heat flux of 2500 W/m², matching the anode thermal boundary condition. This comprehensive set of boundary conditions and parameters enables a coupled multiphysics investigation into the fluid flow, heat transfer, and electrochemical phenomena occurring within the various channels and components of the fuel cell model.

3.3. Mesh Generation and Independence Study

Meshing was performed using ANSYS Workbench 19.2. A structured grid, generated via the Multizone method with controlled edge sizing, was applied to the anode/cathode reactant channels and cooling channels. For the remaining domains, an unstructured mesh utilizing a Patch Conforming algorithm was employed. To enhance the numerical accuracy in resolving electrochemical reactions, grid refinement was implemented specifically through the thickness of the anode/cathode Gas Diffusion Layers (GDLs), Catalyst Layers (CLs), and the Proton Exchange Membrane (PEM). This was achieved by partitioning the GDLs, CLs, and PEM into 5, 4, and 5 grid layers, respectively, across their thicknesses. Laterally, these layers (GDL, CL, PEM) were partitioned into 50 layers. A global element size of 1 mm was defined, with a maximum size of 2 mm and a minimum size constraint (capture tolerance) of 1×10^{-5} mm. The resulting total mesh element count ranged between 1.05 million and 1.90 million. A schematic representation of the mesh is provided in Figure **3**.

In addition, As the generation of the geometry grid should be approached with great attention in order to accurately identify near-wall gradient. In order to satisfy the condition of $y+ \leq 1$, inflated meshes were generated with setting as: initial height of 0.001 mm, height ratio of 1.2, and totally created in 15 layers. Basic mesh quality indicators have been concluded as Table **4**.

To eliminate the potential influence of mesh density on the numerical results, a grid independence study was conducted using Case 3 as the benchmark. The operating conditions for this study were a cooling channel inlet velocity of 1 m/s at 333.15 K, and reactant

Table 4: Mesh Quality Indicators

Terms	Minimum balue	Average value	Maximum value
Orthonology quality	0.745	0.898	0.995
Skewness	0.004	0.102	0.605
Aspect Ratio	1.367	3.342	16.633

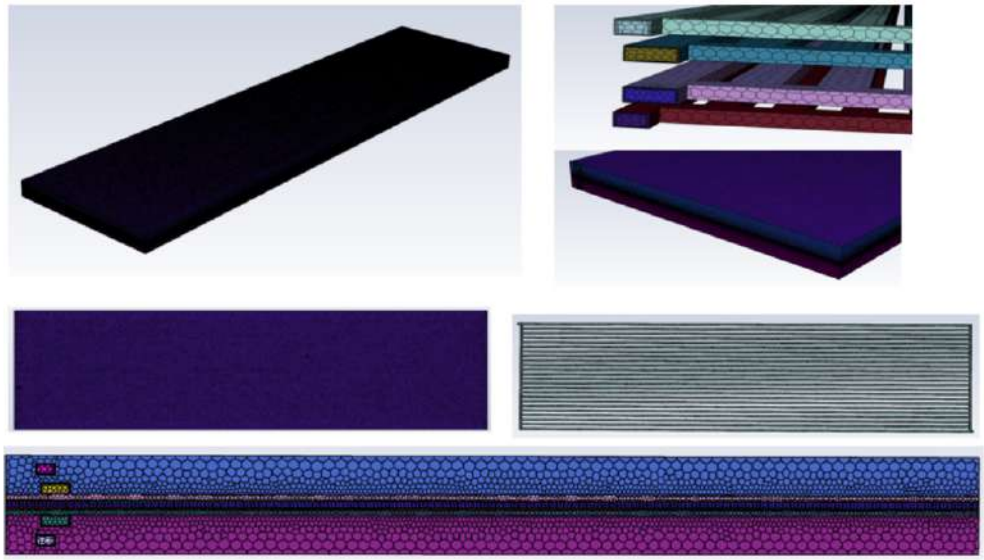

Figure 3: Grid model of the hydrogen fuel cell with parallel reactant flow channels.

channel inlet temperatures of 353.15 K. As observed in Figure **4**, when the mesh element count reached approximately 1.7 million, the difference in the monitored parameters—the inlet-outlet pressure drop and the overall average temperature of the fuel cell—compared to the results from a mesh with approximately 1.8 million elements was less than 3%. Consequently, the meshing strategy yielding around 1.7 million elements was adopted for all subsequent single-cell fuel cell simulations. This approach effectively mitigates grid-induced discrepancies while conserving computational resources.

3.4. Validation of the Numerical Approach

The accuracy and feasibility of the present numerical model were validated against the fuel cell cooling experiments reported in Ref. [28]. A numerical

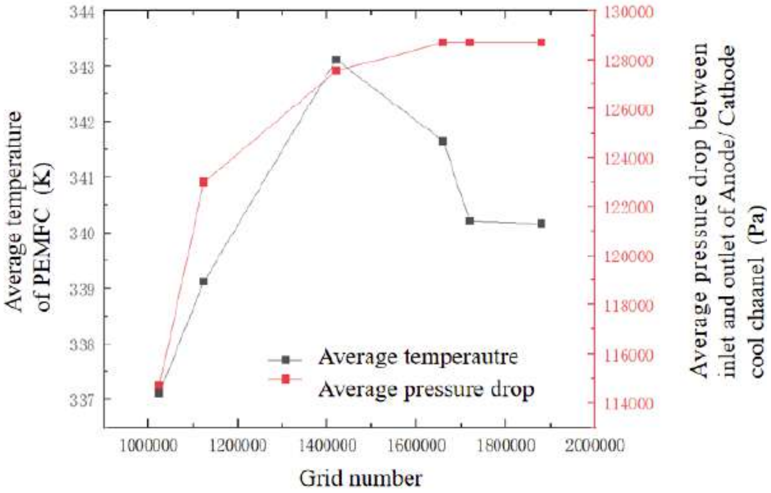

Figure 4: Grid independence study.

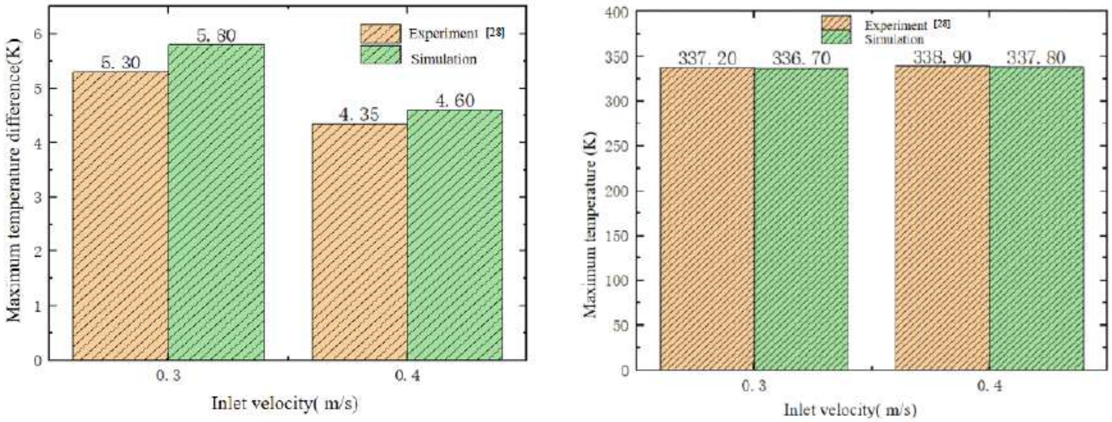

(a) maximum temperature difference on the heated surface

(b) maximum temperature on the heated surface

Figure 5: Numerical model validation by comparing experimental and simulated results.

model featuring a parallel flow channel structure identical to that used in the study—with a channel width of 1 mm and a depth of 0.5 mm—was developed. Simulations were conducted for inlet velocities of 0.3 m/s and 0.4 m/s. The experimental data from Ref. [28] were then compared with the simulation results, as presented in Figure **5**.

It can be observed from Figure **5** that the discrepancy between the experimental and simulated values for the maximum temperature on the heated surface was within 1%. Furthermore, the maximum error in the temperature difference did not exceed 8.2%. These results confirm the reliability of the numerical simulations performed in this work.

4. RESULTS ANALYSIS AND DISCUSSION

4.1. Analysis of the Influence of Reactant Channel Width on Thermal Performance

Figure **6** illustrates the temperature distribution at the interface between the proton exchange membrane and the catalyst layer for different reactant channel width ratios. Significant differences in the temperature distributions are evident among the three width ratios. At a width ratio of 0.02, the temperature distribution is the most uniform, primarily concentrated within a lower temperature range. In contrast, at a width ratio of 0.03, the temperature exhibits a distinct gradient, with lower temperatures near the reactant inlet and higher temperatures further downstream. For a width ratio of 0.04, the temperature distribution is relatively moderate and similar to that at the 0.02 ratio, but the area of the low-temperature transition zone is smaller. These variations in temperature distribution are primarily attributed to the differing reactant channel width ratios, which directly influence the flow patterns, mixing efficiency, and consequently, the extent of the electrochemical reactions. A non-uniform temperature distribution can induce uneven thermal stresses within the fuel cell, adversely affecting its performance and long-term durability. Localized high temperatures may

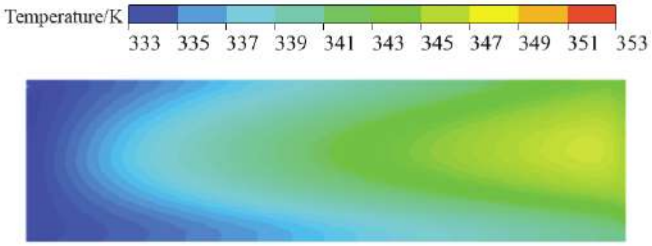

(a) at reactant channel width ratio of 0.02

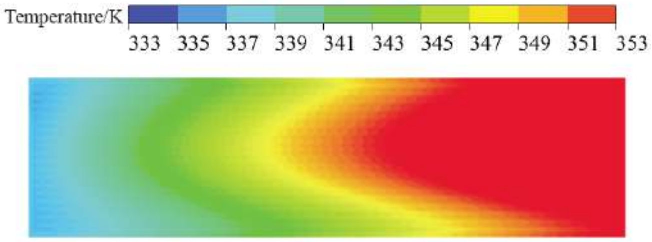

(b) at reactant channel width ratio of 0.03

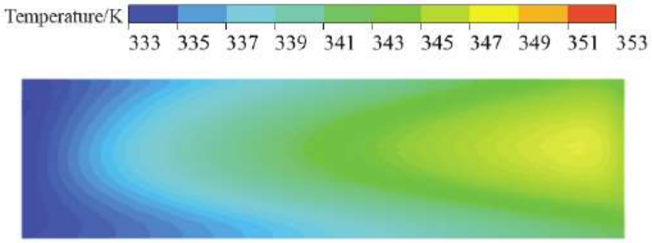

(c) at reactant channel width ratio of 0.04

Figure 6: Temperature contours at the cathode catalyst layer/proton exchange membrane interface under different reactant channel width ratios.

accelerate catalyst degradation and membrane aging, while excessively low temperatures in other regions can lead to insufficient reaction rates, thereby reducing overall efficiency. In summary, the reactant channel width exhibits a complex, non-linear relationship with the overall temperature distribution. Within the parameter range investigated, an optimal value appears to exist, corresponding to a relatively uniform temperature profile that is beneficial for enhancing both the performance and operational stability of the fuel cell. Therefore, optimizing the reactant channel width ratio presents a viable strategy in subsequent research and practical applications to improve the temperature distribution, thereby boosting the performance and extending the lifespan of the fuel cell.

Figure **7** presents a line plot depicting the overall maximum temperature (T_{max}), minimum temperature (T_{min}), and average temperature (T_{avg}) of the fuel cell under different reactant channel width ratios. Analysis of the plot reveals distinct trends associated with the increasing width ratio. Both the maximum and average temperatures exhibit an initial increase followed by a subsequent decrease. In contrast, the minimum temperature demonstrates a more complex, non-monotonic variation. Specifically, as the width ratio increases from 0.020 to 0.030, the maximum and average temperatures rise continuously, peaking at a ratio of 0.03. Over the same interval, the minimum temperature first decreases and then increases. When the width ratio is further increased from 0.030 to 0.040, the maximum and average temperatures show a declining trend, while the minimum temperature again undergoes a decrease followed by an increase. Quantitatively, increasing the width ratio from 0.02 to 0.03 resulted in an approximately 2.96% rise in the maximum temperature and a 2.03% increase in the average temperature. Conversely, increasing the ratio from 0.03 to 0.04 led to decreases of about 3.35% in the maximum temperature and 1.73% in the average temperature. The most significant reduction in the minimum temperature, approximately 2.98%, was observed when the width ratio increased from 0.03 to 0.035. These observed trends can likely be attributed to the influence of the channel width ratio on reactant flow dynamics, mixing efficiency, and consequent reaction rates. A narrower channel promotes higher flow velocity, reducing residence time and potentially limiting the completeness of the electrochemical reaction and its associated heat release. Initially widening the channel slows the flow, extends residence time, allows for more complete reactions, and thus increases heat generation and temperature. This explains the initial rise in both T_{max} and T_{avg}. However, beyond a certain optimal point, an excessively wide channel may lead to poor reactant distribution and localized regions of insufficient reaction, ultimately causing a decline in temperatures in some areas and the observed overall decrease.

The temperature reaches peak value at a width ratio of 0.03. As the channel widens, the gas velocity drops and the residence time of reactants over the catalyst layer increases, raising both conversion and local heat generation. However, once the width exceeds 0.03, the velocity becomes so low that the reactant concentration boundary layer thickens. A quasi-stagnant core then appears in the centre of the channel where species are not effectively consumed; consequently, the areal reaction rate and the associated heat-release rate decline, causing the temperature to fall. In addition, at w_1/W equals 0.03 the competition between in-plane conduction through the rib and convective removal in the channel reaches an optimum. The ribs are still wide enough to provide low-resistance paths that laterally conduct heat toward the cooling channels, while the enlarged channel cross-section simultaneously enhances convective heat removal, preventing local accumulation. When the width ratio is pushed beyond 0.03 the ribs become too narrow: their thermal resistance rises sharply, heat can no longer be efficiently diverted to the coolant, and steeper local temperature gradients appear. The larger thermal load finally imposed on the cooling channels forces an overall temperature drop of the cell.

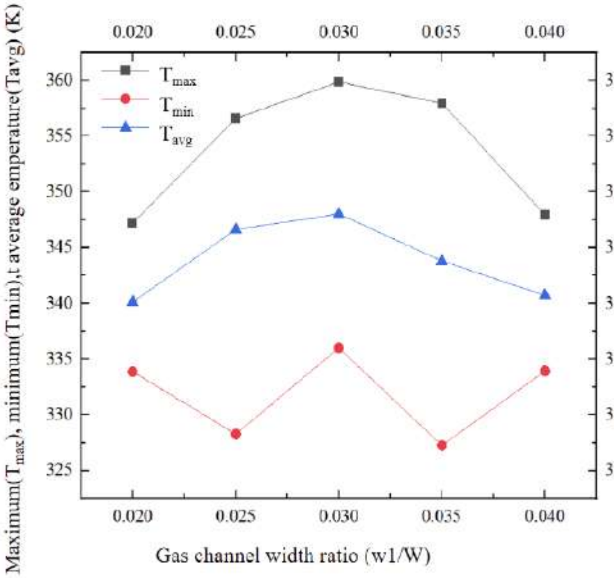

Figure 7: Effect of the reactant channel width ratio on the overall maximum, minimum, and average temperatures.

Figure **8** presents the variations of five distinct temperature differences—namely, the anode reactant channel temperature difference ($\Delta T_{gas\text{-}a}$), cathode reactant channel temperature difference ($\Delta T_{gas\text{-}c}$), anode cooling channel temperature difference ($\Delta T_{cool\text{-}a}$), cathode cooling channel temperature difference ($\Delta T_{cool\text{-}c}$), and the overall temperature difference (ΔT_{entire})—with respect to the reactant channel width ratio. The plot reveals complex, non-linear relationships between all these temperature differences and the width ratio. The inlet-outlet temperature differences across both the anode and cathode reactant channels exhibit a trend of initial decrease followed by an increase, reaching their minimum values near a width ratio of 0.030. Conversely, the temperature differences in the anode and cathode cooling channels show an opposite trend, increasing initially and then decreasing, and peaking near the same width ratio of 0.030. The overall temperature difference displays a more complex, non-monotonic variation, reaching its maximum near a width ratio of 0.035. The variation in reactant channel temperature differences is closely related to the impact of the width ratio on internal heat transfer and electrochemical reaction processes. At a moderate width ratio (e.g., 0.03), reactant flow and reaction are more uniform and complete, leading to concentrated heat release which can result in increased local temperature differences. In contrast, when the width ratio is either too large or too small, alterations in reactant distribution and reaction completeness lead to the observed divergent trends in temperature differences. Furthermore, the cooling channel temperature differences directly reflect their heat exchange capacity. It is evident that the heat removal capability of both the cathode and anode cooling channels is maximized as the width ratio approaches 0.03. This occurs because the most intense electrochemical reactions, and consequently the highest heat generation, take place at this ratio, imposing the most demanding thermal load on the cooling system. This observation corroborates the findings in Figure **7**, where the maximum and average temperatures also peaked at a width ratio of 0.03, indicating the most vigorous electrochemical activity.

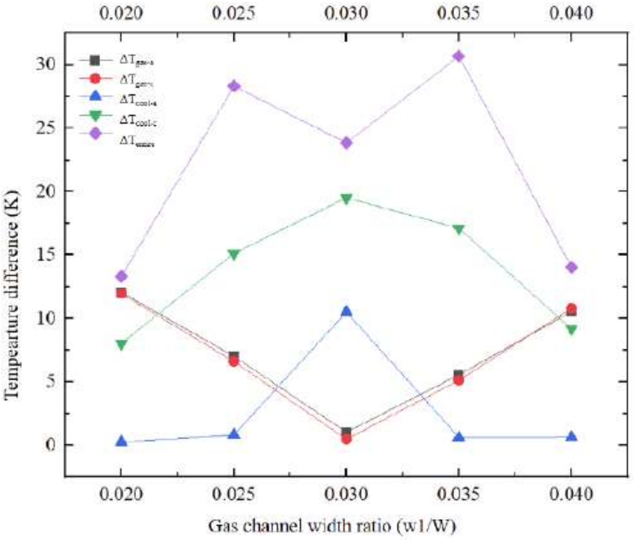

Figure 8: Effect of the reactant channel width ratio on the overall and channel temperature differences.

4.2. Analysis of the Influence of Reactant Channel Height on Thermal Performance

Figure **9** depicts the temperature distribution characteristics at the interface between the proton exchange membrane (PEM) and the cathode catalyst layer under different reactant channel heights. Overall, the reactant channel height exhibits a relatively minor influence on the temperature distribution in this region, with only slight variations observed across the different height configurations. The spacing of the isotherms

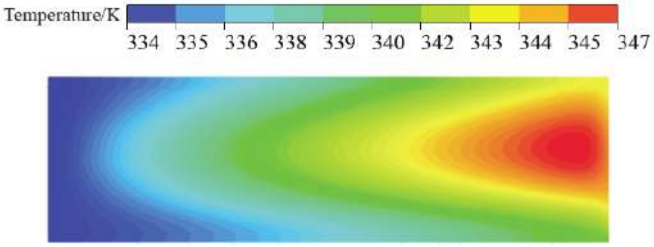

(a) at reactant channel height ratio of 0.25.

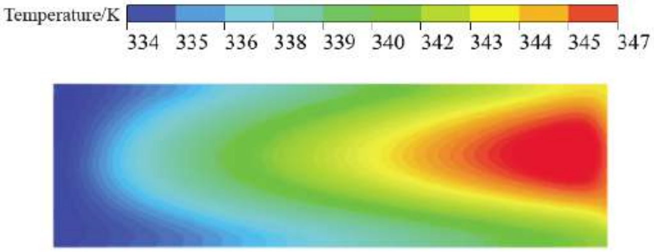

(b) at reactant channel height ratio of 0.3.

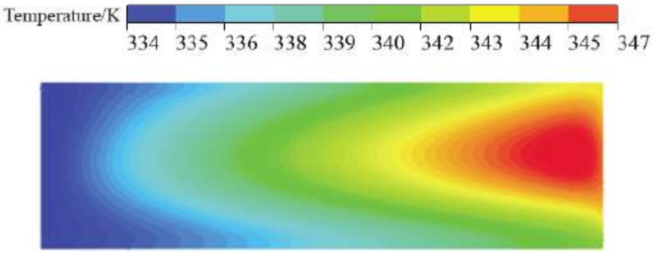

(c) at reactant channel height ratio of 0.35.

Figure 9: Temperature contours at the cathode catalyst layer/proton exchange membrane interface under different reactant channel height ratios.

provides a visual indication of the temperature gradient magnitude. Densely packed isotherms are observed in regions adjacent to the inlets and outlets, signifying more rapid temperature changes and efficient heat exchange during the initial stages of the flow path, where the cooling effect is pronounced. As the coolant progresses along the channel, its temperature gradually increases, leading to a reduced temperature difference relative to the cell components. This diminishes the heat exchange effectiveness, resulting in generally higher temperatures in the downstream sections of the flow path. Comparing the temperature distributions across different height ratios reveals that at a specific ratio of 0.3, the high-temperature zone in the rear section of the PEM/catalyst layer interface is moderately expanded. This suggests that the electrochemical reaction is more intense under this particular height configuration compared to the others investigated.

Figure **10** shows the relationship between the overall maximum temperature ($T_{\max}$), minimum temperature ($T_{\min}$), and average temperature (T_{avg}) of the fuel cell and the variation in reactant channel height ratio. As observed in Figure **10**, when the reactant channel height ratio increases from 0.25 to 0.35, the overall maximum temperature exhibits a slight initial decrease followed by a minor increase, resulting in a net slight decrease of approximately 0.4 K. The magnitude of this fluctuation is relatively low, indicating that adjusting the channel height ratio causes the electrochemical reaction to intensify slightly before weakening slightly again. Similarly, the fluctuations in the overall minimum temperature and average temperature are also minimal, with both decreasing by about 0.2 K over the parameter variation range. This indicates that modifying the reactant channel height has a limited effect on the electrochemical reaction rate of the fuel cell and, consequently, a weak influence on the overall thermal distribution. In summary, the reactant channel height has a minor impact on the maximum, average, and minimum temperatures of the hydrogen fuel cell. This can likely be attributed to the fact that the primary path for heat dissipation within the cell is through the bipolar plate in the width direction, rather than through its height direction.

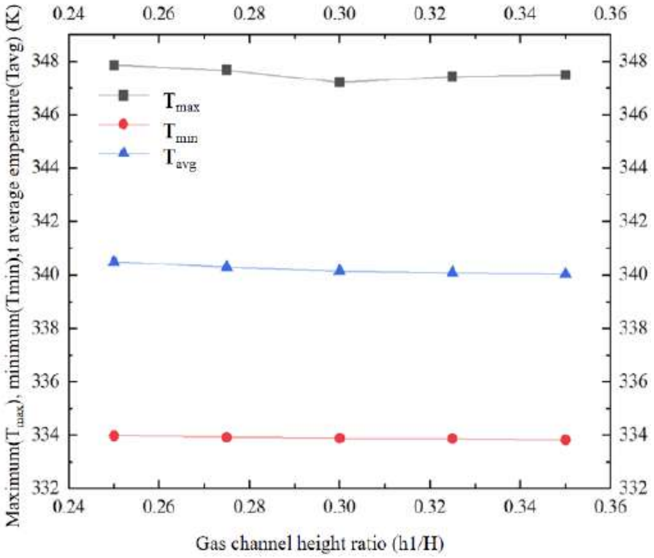

Figure 10: Effect of the reactant channel height ratio on the overall maximum, minimum, and average temperatures.

Figure **11** presents the variation of temperature differences across various channels and the overall system with changes in the reactant channel height ratio. Analysis of Figure **11** indicates that the temperature differences in the reactant channels remain relatively stable overall. The overall temperature difference exhibits a trend of initial increase followed by a decrease as the height ratio increases, with a small fluctuation magnitude and a maximum variation of approximately 0.5 K. The anode reactant channel temperature difference shows a slight increasing trend, rising from about 11.2 K to about 11.8 K (an increase of ~0.6 K), while the cathode reactant channel temperature difference remains largely stable at around 11.5 K. This suggests that as the reactant channel height ratio increases, the heat absorption or release by the reactant gases within the channels changes only marginally. The temperature rise is primarily concentrated in the heat release associated with the reaction process, indicating that alterations in the channel height ratio have a relatively minor impact on the temperature change of the reactant gases themselves. Furthermore, the temperature differences for the anode cooling channel and cathode cooling channel both demonstrate non-linear trends. Specifically, the anode cooling channel temperature difference first decreases and then increases, reaching a minimum value of 0.2 K at a height ratio of 0.3. Conversely, the cathode cooling channel temperature difference first increases and then decreases, peaking at 8.2 K for a height ratio of 0.275. These patterns are related to the influence of the reactant channel height ratio on the internal temperature distribution and electrochemical reaction rates within the fuel cell. When the reactant channel height ratio increases, the vertical distance between the cooling channels and the reactant channels decreases, enhancing the overall heat conduction efficiency. This allows for more thorough heat exchange within the cooling channels. Additionally, the non-linear impact of the increasing reactant channel height ratio on the electrochemical reaction rate, combined with the integrated effect of heat conduction, contributes to these observed results. In summary, within the investigated range of reactant channel height ratios, the overall temperature difference remains at a relatively stable level. This reflects that the thermal management design of the fuel cell system is relatively insensitive to variations in the reactant channel height ratio.

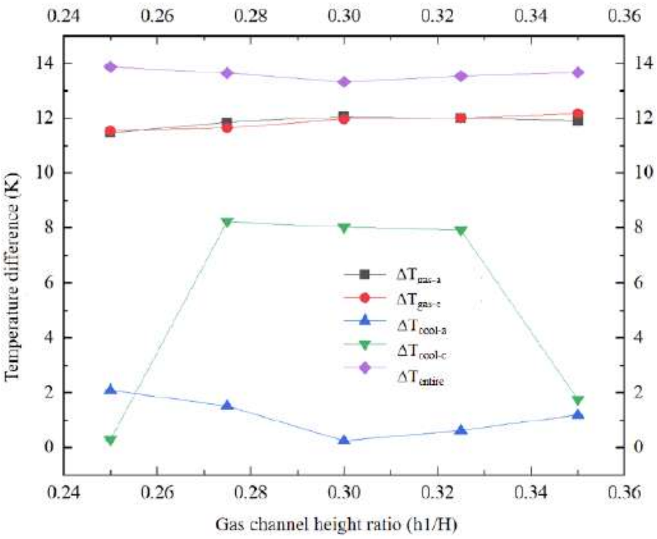

Figure 11: Effect of the reactant channel height ratio on the temperature uniformity of individual channels and the overall cell.

4.3. Analysis of the Influence of Reactant Channel Spacing on Thermal Performance

Figure **12** displays the temperature distribution contours at the interface between the proton exchange membrane (PEM) and the cathode catalyst layer under different reactant channel spacing ratios. Analysis of Figure **12** indicates that the reactant channel spacing ratio has a relatively minor influence on the temperature distribution in this region, with only slight differences observed across the various spacing configurations. The distribution density of the isotherms is similar across the different spacing ratios. In all cases, the isotherms are more densely packed in the low-temperature region near the inlet, exhibiting a distinct layered structure. This dense spacing visually reflects a steeper temperature gradient, indicating more rapid temperature changes and active heat exchange in this zone. As the coolant flows along the channel, its temperature gradually increases, leading to a reduced temperature difference and consequently diminished heat transfer effectiveness. This results in generally higher temperatures in the downstream section, where the isotherms become more sparsely distributed. Locally, at a spacing ratio of 0.02, the stratification within the low-temperature zone is more pronounced compared to ratios of 0.016 and 0.024. This suggests superior heat transfer performance under this specific spacing configuration.

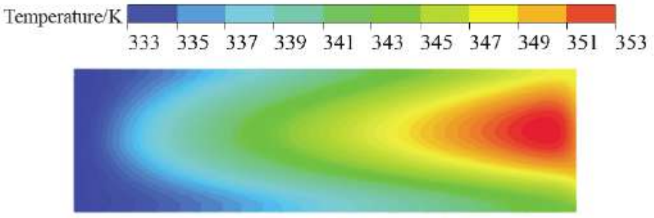

(a) at reactant channel spacing ratio of 0.016.

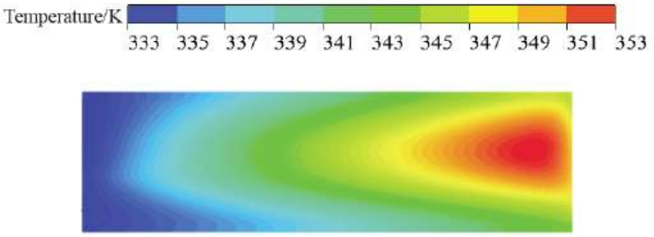

(b) at reactant channel spacing ratio of 0.02.

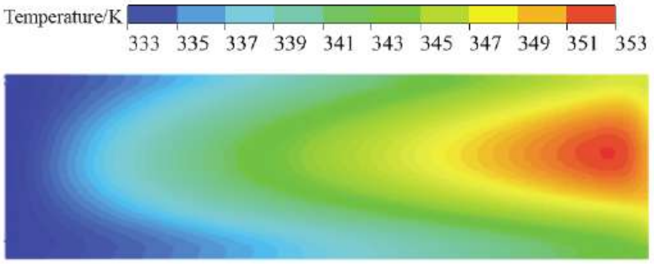

(c) at reactant channel spacing ratio of 0.024.

Figure 12: Temperature contours at the cathode catalyst layer/proton exchange membrane interface under different reactant channel spacing ratios.

Figure **13** illustrates the influence of the reactant channel spacing ratio on the overall maximum temperature (T_{max}), minimum temperature (T_{min}), and average temperature (T_{avg}). As the reactant channel spacing ratio increases from approximately 0.016 to 0.024, the overall maximum temperature of the fuel cell first decreases and then increases, dropping from about 348.2 K to around 347.1 K before rising to 347.5 K. The total temperature fluctuation is 1.1 K, with a relatively small amplitude of about 0.32%. In contrast, the average temperature exhibits a slight decreasing trend, remaining around 340 K overall with a variation of approximately 0.18%. The minimum temperature stays near 334 K, showing minimal change. This phenomenon indicates that increasing the reactant channel spacing ratio has a relatively weak effect on the heat generation and distribution within the fuel cell. Its primary influence is on the electrochemical reaction rate, which consequently affects the maximum temperature, while exerting negligible impact on the overall average temperature and local minimum temperature.

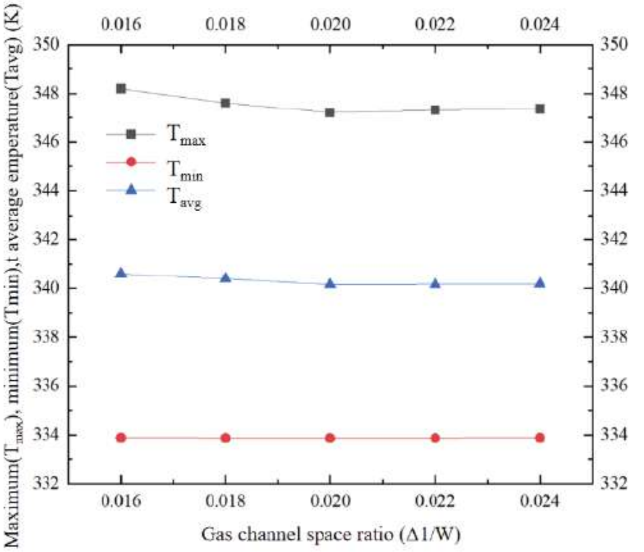

Figure 13: Effect of the reactant channel spacing ratio on the overall maximum, minimum, and average temperatures.

Figure **14** presents the influence of the reactant channel spacing ratio on the temperature uniformity across various channels and the overall system. As observed in Figure **14**, the inlet-outlet temperature differences of the reactant channels remain relatively stable. The temperature differences for both the anode and cathode reactant channels fluctuate within a range of approximately 11.2 K to 12 K. This indicates that variations in the channel spacing have a minor effect on the temperature uniformity of the reactant gases themselves. Interestingly, however, the inlet-outlet temperature differences of the cooling channels exhibit significant variation. The temperature difference of the cathode cooling channel initially increases from 2.4 K to approximately 8 K and then decreases to 2.3 K as the spacing ratio increases, representing a maximum variation of 5.6 K. Conversely, the temperature difference of the anode cooling channel decreases from about 2.6 K to 0.2 K before rising slightly to 1.8 K, with a maximum variation of 2.4 K. This suggests that the temperature rise of the coolant is highly sensitive to changes in the reactant channel spacing. This phenomenon may originate from the adjustment of the channel spacing, which alters the overall distribution of the cooling load. This redistribution induces changes in the global temperature field, consequently affecting the thermophysical properties of the coolant and ultimately influencing its flow distribution and pressure drop characteristics across the cooling channels. Furthermore, the overall temperature difference remains largely constant at around 14 K across the entire range of spacing ratios, showing only a slight decreasing trend. This further confirms that modifying the reactant channel spacing has a limited effect on the overall thermal management efficacy of the fuel cell.

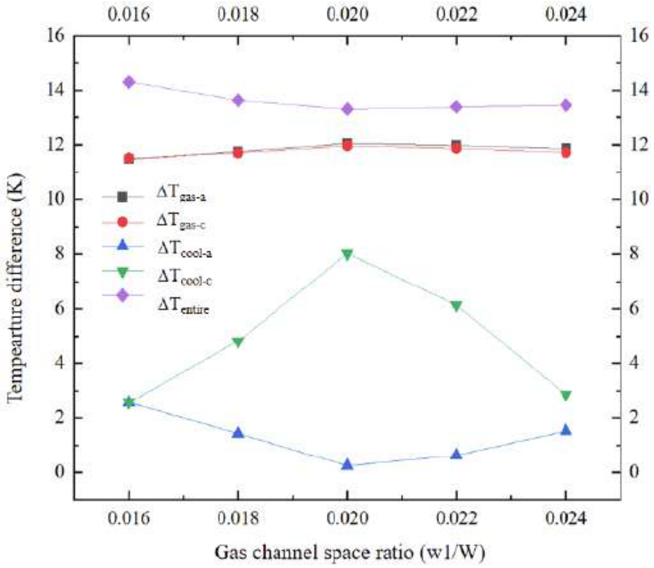

Figure 14: Effect of the reactant channel spacing ratio on the temperature uniformity of individual channels and the overall cell.

4.4. Comprehensive Discussion

Based on the aforementioned research findings, key engineering insights directly relevant to UAV design requirements are derived as follows:

Firstly, the identification and management of high-temperature risk zones form the foundation for ensuring UAV thermal safety and extended endurance. The results presented in Sections 4.1 to 4.3 clearly indicate a triangular high-temperature region near the reactant channel outlets. Furthermore, specific ranges of the reactant channel width ratio (0.03-0.035) were found to induce peak temperatures and maximum temperature differences. These areas distinctly pinpoint potential thermal runaway risks during fuel cell operation. Consequently, in engineering design, it is imperative to eliminate these thermal hotspots through further optimization of the flow field layout and enhancement of local heat dissipation. This approach is crucial for elevating the thermal safety margin and operational reliability of the UAV system, thereby ensuring superior performance in prolonged missions.

Secondly, the implementation of an asymmetric and energy-efficient thermal management strategy is key to improving the sustainable flight efficiency of UAVs. The findings in Sections 4.1 to 4.3 unequivocally demonstrate that the cathode side bears the vast majority of the heat dissipation load. This necessitates abandoning traditional symmetric design philosophies for the thermal management system. By implementing targeted, enhanced cooling specifically on the cathode side, waste heat can be removed with maximum efficiency. This strategy maintains the hydrogen fuel cell within its optimal operating temperature range while simultaneously minimizing the power consumption of the cooling system itself. The resultant improvement in the net power output directly enhances UAV endurance and sustainable flight efficiency.

Finally, leveraging the design freedom offered by key geometric parameters provides an effective pathway towards achieving UAV system lightweighting and compactness, ultimately boosting flight efficiency. The results discussed in Sections 4.2 and 4.3 reveal that the reactant channel height ratio and spacing ratio have negligible impact on the fuel cell's maximum, average, and minimum temperatures, as well as on the overall and reactant channel temperature differences. This implies that engineers possess significant flexibility to adjust these parameters without compromising the core electrochemical performance of the cell. This freedom can be strategically utilized to optimize the design for reduced weight and more compact integration. For UAVs, which operate under stringent weight and space constraints, this represents a critical technological pathway for integrating high-power-density propulsion systems and achieving high sustainable flight efficiency.

5. CONCLUSIONS AND FUTURE WORK

Numerical simulations were conducted to analyze the influence of structural parameters in parallel reactant flow channels on the heat transfer characteristics of bipolar plates for UAV-applicable hydrogen fuel cells. The main conclusions are as follows:

(1) The lowest fuel cell temperatures are observed at the reactant channel inlets and along the two lateral sides of the cell. In contrast, higher temperatures are found near the reactant channel outlets, forming a distinct triangular-shaped high-temperature zone.

(2) As the reactant channel width ratio increases from 0.02 to 0.04, both the maximum and average temperatures of the fuel cell exhibit a pattern of initial increase followed by a decrease. All three key temperature metrics—maximum, minimum, and average temperature—reach their peak values at a width ratio of 0.03.

(3) The temperature differences in both the anode and cathode reactant channels demonstrate a trend of initial decrease followed by an increase with rising width ratio, reaching their minimum values at a width ratio of 0.03. Conversely, the temperature differences in the anode and cathode cooling channels show an opposite trend, increasing initially and then decreasing, and peaking at the same width ratio of 0.03. The overall temperature difference of the cell reaches its maximum near a width ratio of 0.035.

(4) Under different reactant channel height ratios and spacing ratios, the temperature differences across the cathode and anode reactant channels are nearly identical. However, the temperature difference in the cathode cooling channel (maximum approximately 8 K) is consistently greater than that in the anode cooling channel (maximum approximately 2 K).

(5) The reactant channel height ratio and spacing ratio exhibit negligible effects on the maximum, average, and minimum temperatures, the overall temperature difference, and the reactant channel temperature differences of the fuel cell. However, they significantly influence the temperature differences within the cooling channels.

Based on the above research results, our engineering recommendations are as follows: it is recommended to set the width ratio of the reactant flow channel outside the range of 0.03-0.035 in the thermal management design of hydrogen fuel cells for UAV to avoid the highest operating temperature, and prioritize the use of asymmetric enhanced cooling strategies for the cathode side. At the same time, height ratio and spacing ratio of the reactant flow channels can be used as regulating variables to achieve the integration of lightweight and compact fuel cells of UAV Applications.

Building upon this research, future work will focus on investigating the effects of structural parameters in serpentine reactant channels and serpentine cooling channels on the heat transfer performance of fuel cell bipolar plates. Furthermore, by integrating the analysis with varying UAV operational conditions, a comprehensive study will be performed to evaluate the heat transfer and electrochemical performance of fuel cells with different reactant and cooling channel configurations. The ultimate objective is to identify the optimal types and structural parameters for reactant and cooling channels tailored specifically for dynamic UAV operating environments.

ACKNOWLEDGEMENTS

This research was funded by the Key Science and Technology Research and Development Project of Shaanxi Provincial Administration for Market Regulation (40120240331) and the Xi'an Jiaotong University Basic Research Business Fee Free Exploration Project (xzy012023071).

REFERENCES

[1] Shamsizadeh P, Ziaei-Rad M, Afshari E. Simulation of proton exchange membrane fuel cell cooling plates under different heat fluxes. Appl Therm Eng 2025; 127759. https://doi.org/10.1016/j.applthermaleng.2025.127759

[2] Zhao J, Cheng X, Zhong Z, Ma Y, Zhou C, Lv Y, Li C. Thermal characteristics analysis of a novel vapor chamber suitable for air-cooled PEMFC thermal management. Int J Heat Mass Tran 2025; 253: 127575. https://doi.org/10.1016/j.ijheatmasstransfer.2025.127575

[3] Jiang Q, Xiong S, Sun B, Chen P, Chen H, Zhu S. Research on energy-saving control of automotive PEMFC thermal management system based on optimal operating temperature tracking. Energies 2025; 18(15): 4100. https://doi.org/10.3390/en18154100

[4] El Idi MM, Ankouni M, Slama RBH, Nobrega PA, Hajjar A, Atli A. Critical review of the latest advances in thermal management techniques for PEM fuel cells. Renew Sust Energ Rev 2026; 226: 116199. https://doi.org/10.1016/j.rser.2025.116199

[5] Sasmito AP, Kurnia JC, Mujumdar A S. Numerical evaluation of various gas and coolant channel designs for high performance liquid-cooled proton exchange membrane fuel cell stacks. Energy 2012; 44(1): 278-291. https://doi.org/10.1016/j.energy.2012.06.030

[6] Afshari E, Ziaei-Rad M, Dehkordi MM. Numerical investigation on a novel zigzag-shaped flow channel design for cooling plates of PEM fuel cells. J Energ Inst 2017; 90(5): 752-763. https://doi.org/10.1016/j.joei.2016.07.002

[7] Joibary SMM, Rahgoshay S, Rahimi-Esbo M, Firouzjaee KD. Numerical investigation of the influence of different cooling flow channels on the thermal and water saturation distribution in a real dimensional polymer electrolyte membrane fuel cell. Int J Hydrogen Energ 2023; 48(7): 2762-2787. https://doi.org/10.1016/j.ijhydene.2022.09.260

[8] Li S, Sunden B. Numerical analysis on thermal performance of cooling plates with wavy channels in PEM fuel cells. Int J Numer Method H 2018; 28(7): 1684-1697. https://doi.org/10.1108/HFF-01-2018-0034

[9] Peng C, Gu H, Zhang G, Luo K, Xu P, Lv S, Zhang Q, Chen G. Numerical study on heat transfer enhancement of a proton exchange membrane fuel cell with the dimpled cooling channel. Int J Hydrogen Energ 2023; 48(8): 3122-3134. https://doi.org/10.1016/j.ijhydene.2022.10.136

[10] Xia L, Yu Z, Xu G, Ji S, Sun B. Design and optimization of a novel composite bionic flow field structure using three-dimensional multiphase computational fluid dynamic method for proton exchange membrane fuel cell. Energ Convers Manage 2021; 247: 114707. https://doi.org/10.1016/j.enconman.2021.114707

[11] Yao A, Cao Y, Liu D, Yu L. Research of hydrothermal management characteristics of proton exchange membrane fuel cell. Chin J Power Sources 2023; 47(3): 341-347. https://doi.org/10.3969/j.issn.1002-087X.2023.03.01

[12] Shen J, Tu Z, Chan S. Evaluation criterion of different flow field patterns in a proton exchange membrane fuel cell. Energ Convers Manage 2020; 213: 112841. https://doi.org/10.1016/j.enconman.2020.112841

[13] Liao Z, Wei L, Dafalla A M, Guo J, Jiang F. Analysis of the impact of flow field arrangement on the performance of PEMFC with zigzag-shaped channels. Int J Heat Mass Tran 2021; 181: 121900. https://doi.org/10.1016/j.ijheatmasstransfer.2021.121900

[14] Najmi AUH, Anyanwu IS, Xie X, Liu Z. Experimental investigation and optimization of proton exchange membrane fuel cell using different flow fields. Energy 2021; 217: 119313. https://doi.org/10.1016/j.energy.2020.119313

[15] Alizadeh E, Rahimi-Esbo M, Rahgoshay SM, Saadat SHM, Khorshidian M. Numerical and experimental investigation of cascade type serpentine flow field of reactant gases for improving performance of PEM fuel cell. Int J Hydrogen Energ 2017; 42(21): 14708-14724. https://doi.org/10.1016/j.ijhydene.2017.04.212

[16] Qin Z, Huo W, Bao Z, Tongsh C, Wang B, Du Q, Jiao K. Alternating flow field design improves the performance of proton exchange membrane fuel cells. Adv Sci 2023; 10(4): 2205305. https://doi.org/10.1002/advs.202205305

[17] Zuo Q, Li Q, Chen W, Peng R, Zhu X, Xie Y, Yang X. Optimization of blocked flow field performance of proton exchange membrane fuel cell with auxiliary channels. Int J Hydrogen Energ 2022; 47(94): 39943-39960. https://doi.org/10.1016/j.ijhydene.2022.09.143

[18] Min C, Li F, Gao X, Wang K, Rao Z. Secondary flow on the performance of PEMFC with blocks in the serpentine flow field. Int J Hydrogen Energ 2022; 47(67): 28945-28955. https://doi.org/10.1016/j.ijhydene.2022.06.191

[19] Chen H, Guo H, Ye F, Ma C. An experimental study of cell performance and pressure drop of proton exchange membrane fuel cells with baffled flow channels. J Power Sources 2020; 472: 228456. https://doi.org/10.1016/j.jpowsour.2020.228456

[20] Lu G, Fan W, Lu D, Zhao T, Wu Q, Liu M, Liu Z. Lung-inspired hybrid flow field to enhance PEMFC performance: A case of dual optimization by response surface and artificial intelligence. Appl Energ 2024; 355: 122255. https://doi.org/10.1016/j.apenergy.2023.122255

[21] Atyabi SA, Afshari E, Shakarami N. Three-dimensional multiphase modeling of the performance of an open-cathode PEM fuel cell with additional cooling channels. Energy 2023; 263: 125507. https://doi.org/10.1016/j.energy.2022.125507

[22] Carcadea E, Varlam M, Ismail M, Ingham DB, Marinoiu A, Raceanu M, Ion-Ebrasu D. PEM fuel cell performance improvement through numerical optimization of the parameters of the porous layers. Int J Hydrogen Energ 2020; 45(14): 7968-7980. https://doi.org/10.1016/j.ijhydene.2019.08.219

[23] Shen J, Xu L, Chang H, Tu Z, Chan S. Partial flooding and its effect on the performance of a proton exchange membrane fuel cell. Energ Convers Manage 2020; 207: 112537. https://doi.org/10.1016/j.enconman.2020.112537

[24] Peng P, Mahyari H M, Moshfegh A, Javadzadegan A, Toghraie D, Shams M, Rostami S. A transient heat and mass transfer CFD simulation for proton exchange membrane fuel cells (PEMFC) with a dead-ended anode channel. Int Commun Heat Mass 2020; 115: 104638. https://doi.org/10.1016/j.icheatmasstransfer.2020.104638

[25] Chen X, Yu Z, Yang C, Chen Y, Jin C, Ding Y, Wan Z. Performance investigation on a novel 3D wave flow channel design for PEMFC. Int J Hydrogen Energ 2021; 46(19): 11127-11139. https://doi.org/10.1016/j.ijhydene.2020.06.057

[26] Atyabi SA, Afshari E. Three-dimensional multiphase model of proton exchange membrane fuel cell with honeycomb flow field at the cathode side. J Clean Prod 2019; 214: 738-748. https://doi.org/10.1016/j.jclepro.2018.12.293

[27] Li J, Gao J, Xu L, Xi L, Liang F, Zhou Y, Ran H, Lin H, Yang T, Li Y. Investigation on Thermal Management Enhancement in Proton Exchange Membrane Hydrogen Fuel Cell Based on Cooling Channels Design with Bathtub-Shaped Turbulators. Renew Energ 2026; 256: 124720. https://doi.org/10.1016/j.renene.2025.124720

[28] Han K, Tang J, Zhang J, Su J. Structural optimization of cooling channels for 2 kW fuel cells. J Hefei Univ Technol (Nat Sci) 2020; 43(8): 5. https://doi.org/10.3969/j.issn.1003-5060.2020.08.007